

THE CLOUD-BASED IMPLEMENTATION AND STANDARDIZATION OF ANTHROPOMORPHIC PHANTOMS AND THEIR APPLICATIONS

Osiris Núñez-Chongo
Manuel Carretero

Rafael Mayo-García

Gregorio Millán Institute for Fluid Dynamics,
Nanoscience and Industrial Mathematics
Department of Mathematics,
Universidad Carlos III de Madrid
Av. de la Universidad 30, Leganes, 28911, SPAIN

Technology Department
Centro de Investigaciones Energéticas,
Medioambientales y Tecnológicas (CIEMAT)
Av. Complutense 40, Madrid, 28040, SPAIN

Hernán Asorey

Medical Physics Department
Comisión Nacional de Energía Atómica
Centro Atómico Bariloche,
San Carlos de Bariloche, 8400, ARGENTINA

ABSTRACT

Radiation protection applications often require the creation of a large number of precise simulations of radiation-human body interactions. Our research is focused on creating `RadPhantom`, a new Geant4 application that constructs voxelized anthropomorphic phantom models. This allows for the standardized and reproducible generation of Geant4 simulations in cloud-based environments. We have incorporated existing and publicly accessible models into Meiga, a framework designed for the integration of Geant4-based applications. To standardize these simulations, guarantee their reproducibility, and adhere to the FAIR principles, we have developed an extended vocabulary schema using metadata and ontologies that align with current standards. By employing virtualization containers, we capitalize on the scalability and adaptability of public and federated clouds. In this paper, we detail our implementation, present some benchmarking results and comparisons with current methodologies, and discuss the potential applications for evaluating doses on commercial flights or assessing radiation shielding in neutron production facilities.

1 INTRODUCTION

To precisely forecast the effects of ionizing radiation on living organisms, a comprehensive model of particle transport and radiation interactions in biomaterials needs to be developed. This model must be constructed by accounting for various combinations of factors such as different tissues, types of radiation, and incident radiation energies/spectra. Additionally, incident radiation geometries and molecular reaction effects produced by different species should be considered.

In this context, computational human phantoms are extensively used in medical physics applications to estimate the dose within human tissues and organs resulting from specific radiation environments. The computational human phantoms were initially developed as a series of analytic phantom models, which constructed the internal organs and boundaries of the phantom using simple geometries such as planes, cylinders, spheres, cones, elliptical cylinders, and ellipsoids (Clement 2009; Dewji et al. 2004; Guatelli

et al. 2006). Despite their lack of anatomical realism, these reference models have been used to provide consistent and reproducible radio-protection guidance for different types of exposures.

In recent years, medical imaging technologies have advanced, providing high-resolution cross-sectional digital images that allow for enhanced anatomical structure representation. Currently, human voxelized models are designed based on these techniques, where a numeric index, material, and placement inside the phantom are associated with each generated voxel. One main issue of voxelization is the overestimation of the mass and size of small structures when they are smaller than the voxel dimensions. In addition, organs with spherical approximations can also have overestimated surface areas, and the organ positions and shapes can vary depending on the position of the person, standing, sitting, or lying as the most common ones. Ongoing refinement of voxel phantoms aims to provide increasingly accurate human anatomy representation, allowing for more realistic estimations of organ doses in organs (Caon 2004).

For accurate simulation of radioactive transport problems in these complex geometries and in a variety of different types of materials and densities, Monte Carlo (MC) simulations are performed. MC tracking codes are essential tools for investigating radiation effects at various spatial and energy scales (Sempau 2002). Some radiation transport codes have integrated different voxel phantom models in the past (Sato et al. 2007; Martins et al. 2014; Franck et al. 2001; Costa et al. 2015). However, previous voxel phantom implementations are generally unavailable to the public.

Among the various codes available, the Geant4 Monte Carlo simulation toolkit (Agostinelli et al. 2003) offers a general platform for radiation-matter interactions simulation and an approach for the development of accurate dose calculation applications (Sarrut et al. 2022). Its hierarchical structure includes a set of components for geometric description, particle definition, navigation and tracking, electromagnetic fields, physical models for interactions (electromagnetic, hadronic, optical, photo-nuclear, and electro-nuclear), event scoring, visualization, and component management software (Allison et al. 2016). This software is widely used due to its continuous improvements, its simulation performance, refinement of physical models, enhancement of its capabilities, and its open-source strategy.

In the field of Geant4-based applications, our group is developing Meiga, a package of tools that allow for the integration of simulations in Geant4, sophisticated description of geometry, advanced 3D visualization tools, and validated physical models. The purpose of this work is to create a new application for calculating the effects of radiation on human anatomy *in-silico* by leveraging and extending Meiga capabilities. The Recommendation 110 of the International Commission on Radiological Protection (ICRP) has introduced voxelized anthropomorphic phantoms for adult males and females, which are now becoming the official computational models representing the adult Reference Male and Reference Female (Clement 2009). To achieve this purpose, we have faced some challenges. Improving the spatial resolution of simulations by reducing voxel size, for example, comes with the challenge of mitigating the consequent computational demands resulting from an increased number of voxels. This has been achieved by the utilization of virtualized containers. By encapsulating the application and its dependencies, it becomes feasible to harness the vast computational resources offered by large high-performance computing (HPC) facilities and public and federated clouds, such as the European Open Science Cloud (ESOC). Standardized computational mechanisms are crucial for maximizing the benefits of the simulation framework, particularly for coordinating, sharing and curating results. In this work, we present RadPhantom, a new application that allows, e.g., the evaluation of radio- and hadrontherapy doses, as well as determining, e.g., the effective dose received by a person exposed to high radiation environments, such as those encountered onboard commercial flights or inside rapid-neutron production facilities.

2 MATERIAL AND METHODS

2.1 Structure of the Meiga Framework

Meiga is a software framework based on Geant4 and designed was originally designed to facilitate the calculation of particle transport over hundreds or thousands of meters of rock with varying densities and

compositions (Taboada et al. 2022), as well as for the design and characterization of particle detectors for muography (Taboada et al. 2022; Calderón-Ardila et al. 2022). This new technique allows for the estimation of the spatial distribution of the density of large objects, such as an active volcano, by taking advantage of the high penetration capacity of high-energy atmospheric prompt muons (Tanaka 2022; Rubio-Montero et al. 2021). The framework consists of a range of C++ classes, each serving a specific function. It achieves this through the integration of Geant4 simulations, which perform the particle transport and calculate the detector response. Geant4 is utilized as an external toolkit, and Meiga provides the necessary interfaces for users to access detector descriptions and run managers. Meiga includes a variety of customizable applications that enable non-experts to run and access simulated data by using configuration files written using the XML and JSON standards. These customizable applications allow users to tailor the framework to their specific needs (Taboada et al. 2022).

The original Meiga's workflow is based on three consecutive steps. The first step consists of the injection of the high-energy flux of secondary particles. These particles are produced during the interaction of energetic cosmic rays with the atmosphere, producing the atmospheric background radiation, mainly composed of electromagnetic particles (e^\pm and γ), muons (μ^\pm), and hadrons (mainly p , n , π^\pm). From those, only a small fraction of muons possesses enough energy to traverse across hundreds or even thousands of meters of rock. Depending on the geometry and the density profile of the studied object, the minimum muon energy could even be up to hundreds of GeV (Rubio-Montero et al. 2021; Bertolli et al. 2022). Meiga includes the EcoMug library (Pagano et al. 2021) for a fast generation of samples of atmospheric muons. However, for obtaining a more accurate distribution of the expected atmospheric flux at the site, Meiga includes a module for handling the secondary particles file produced by ARTI, a publicly available framework, developed for the precise calculation of the atmospheric background in any place of the World and under realistic and real-time atmospheric and geomagnetic conditions (Sarmiento-Cano et al. 2022), and including the high-energy components of the muon flux (Rubio-Montero et al. 2021).

Once the flux is injected, propagation through the ground takes place. Different and consecutive layers of rock can be modeled. The final step is to simulate the response of the detector. For this matter, Meiga includes different types of detectors typically used in high-energy particle physics.

The top level of Meiga's hierarchical structure is the `Event`, which sets the workflow during execution. This structure defines variables that describe the detector and the simulation data, and a connection is established between them. The `Detector` class provides an interface to the `Event`, from which the detector's description can be read. Once the simulation is executed, the input file containing the data is read and stored in the `Event`. They share the detector implementation, physics conditions, and secondary generation or input. The process starts by invoking the set mandatory user initialization classes, which set the simulation options from the `Event`. The detector geometry, materials used in its construction, selection of all physics processes to be simulated, and the definition of primary particles are configured. This setup can be done manually, or automatically using predefined detector models and physics lists that are contained in the `G4Models` class. Simulation data is stored in two ways: using user hooks, where the information extracted from simulations is stored in the `SimData` class, and using the built-in scoring commands available in Geant4. Data can be accessed at the event and detector levels through the `SimData` class. Similarly, the command-based scoring functionality allows for the collection of data from simulations. Further details, including the MEIGA class descriptions and a simplified schema of the Meiga simulation workflow, are presented in the original publication (Taboada et al. 2022).

The Meiga framework incorporates a set of utilities, including a parser of configuration files, physics constants, and geometry and mathematical calculations. The use of standardized configuration file formats such as JSON and XML facilitates the exchange of simulation settings and data with other applications and even supports the standardization of the production of digital twins. One of the benefits of using the modular and extensible design of Meiga is that it provides a set of predefined detector models and physics lists, which can be easily extended or modified to suit the user's needs. These models and lists can be used as a starting point to develop custom detectors and physics processes, saving the user significant

development time and effort. To accomplish this, the new classes developed inherit properties and methods from the classes provided in the framework. For instance, new detector classes can be created by inheriting from the `Detector` class or new materials can be defined in the `Materials` class. Additionally, new action classes can be created to perform additional tasks during the simulation.

2.2 The implementation of anthropomorphic phantoms in Meiga

A new application, named `RadPhantom`, has been developed within our computational framework by harnessing the extension capabilities of `Meiga`. This application enables the modeling of the interaction between radiation and a computational model of the human body. Following the recommendations of the ICRP110 publication (Clement 2009), two models of an anthropomorphic voxelized phantom were generated in two manners: (a) by voxelizing the geometry from DICOM images and (b) by creating a mesh based on the Adult Male and Female reference computer models defined in the ICRP110 publication (Large et al. 2020). The main sources from the ICRP110 adult reference voxel phantoms, which are included as two advanced examples in the `Geant4` application, `DicomG4` and `human-phantom`, were adapted to build this application (Large et al. 2020). Two CT scans were respectively acquired from a male and a female subject in a supine position with the arms parallel to the body, as shown in Figure 1. The main characteristics of the ICRP110 Adult Reference Computational Phantom can be found in Table 1 of (Large et al. 2020) for reference. In the first trials, the original slices of 512x512 pixels were reduced to 64x64 voxels to reduce the computational cost.

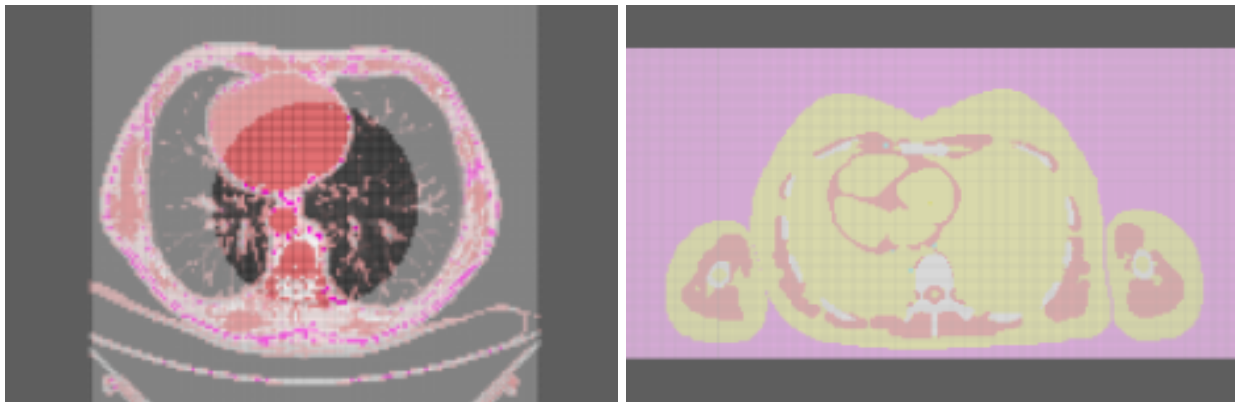


Figure 1: A section of the anthropomorphic phantoms adapted for `RadPhantom`: the `DicomG4` reference model (left), and visualization the voxelized female phantom from the `human-phantom` examples in the slice number 265 (right).

The initialization and construction of the phantoms are performed in the constructor of the `Detector` class, as explained in subsection 2.1. This class extracts the information from the new `Event` structure. The `world` is a cube with a volume of 2m^3 filled with dry air. Depending on the user's input, the corresponding phantom model (DICOM or ICRP110 mode) is selected. Consequently, a set of methods adapted from each model imports information from the corresponding ASCII files `DICOMData.dat`, `FemaleData.dat`, or `MaleData.dat`. These files contain information about the 142 organs and the corresponding 53 building materials associated with each voxel, including those filled with air.

Furthermore, a specialized method was developed to accommodate varying voxel sizes and the corresponding number of voxels for specific applications. As in the original implementation, voxel data and corresponding material IDs are stored in a dedicated array before constructing a parameterized volume using the `Geant4` Nested Parameterization functionality. This approach utilizes a nested strategy that eliminates gaps between different voxels. The material composition of each voxel varies according to its position. Instead of employing a direct three-dimensional parameterized volume, the first (sagittal) and

second (coronal) axes are sequentially replicated, followed by one-dimensional parameterization along the third axis (axial). This strategy improves memory access and consumption for geometry optimization and enables faster navigation through the large number of voxels present in the model. The dose information observed at each voxel is recorded in a JSON file for further analysis using the available analysis tools in Meiga. Additionally, this file, together with the input JSON file, undergoes processing to generate the corresponding metadata, which will be further discussed in the subsequent subsection.

2.3 Standardizing the RadPhantom Application

To achieve precise and accurate results of radiation interaction with matter, significant computational resources are required, which are becoming more widely available as computing and storage capabilities continue to grow. However, there remains a pressing need to standardize the production, analysis, curation, and access of synthetic, and eventually measured, data. Recent efforts have therefore focused on integrating and standardizing our astroparticle and muography simulation and data analysis codes within the European Open Science Cloud (EOSC) ecosystem (Rubio-Montero et al. 2021).

The integration of application codes aims to establish a framework for defining, generating, and storing data and metadata using tools that can be deployed in virtualized and containerized environments based on Docker images (Rubio-Montero et al. 2021). These efforts are expected to facilitate data sharing and promote collaboration by adopting the Open Science paradigm with the FAIR (Findable, Accessible, Interoperable, Re-usable data) principles, as well as the federation of virtual resources and organizations. The utilization of Docker images enables the sharing of tools and workflows, thereby enhancing the reproducibility of results.

To simulate radiation-matter interactions in an anthropomorphic phantom within the Meiga framework, we have implemented a cloud-based production system. This system is fully integrated by deploying the new RadPhantom docker container on a limited set of cloud resources provisioned by EOSC. The docker container encompasses all the necessary dependencies of the Meiga framework, including ROOT (a data-analysis framework) (Brun and Rademakers 1997), Geant4, and the relevant parsers for XML and JSON files.

For building this production computing virtual facility, we followed the same schema explained in (Rubio-Montero et al. 2021), including the utilization of several EOSC- and EGI-based services: **Geant EduTeams** and **EGI Check-in** as the primary identity providers for accessing the resources, **EGI DataHub** as the main cloud-storage service based on OneData, a globally distributed cloud file system that enables various ways of accessing and sharing data and metadata, and the Infrastructure Manager (IM) from the **EGI Check-in** service. For this work, we established a virtual cluster based on a Slurm Workload Manager job scheduler with one virtual master (*v-master*) and 8 *v-nodes*, each equipped with 8 Intel Xeon Core E7 processors, and 250 GB of shared memory and disk each. We configured Docker to use both unified and equally as needed. Furthermore, we included a local version of the public MEGA storage service for possible users who do not have access to the EOSC services. This provides a secure, cloud-based exchange repository for the configuration input files and storage of the resulting outputs.

Standardized schemes based on linked data have become increasingly prevalent in the trend towards Open Data. To follow this direction, we decided to utilize standardized schemes for the metadata of this application due to their simplicity and compatibility. Specifically, we defined the metadata using JSON-LD 1.1 (W3C), a language syntax now promoted by the big players of the sector, such as Google, that is becoming the standard replacement for heavier syntaxes like RDF/XML or Turtle. The main vocabulary used in this application is DCAT-AP2, which is a specific profile of DCAT2 (W3C) recommended for repositories, content aggregators, or data consumers related to the public sector. Furthermore, we utilized the RadiationTherapy class in schema.org (Brickley et al. 2022) to describe the synthetic data generated in each irradiation simulation. This includes information such as the treatment modality, radiation type, and target anatomy.

In addition to utilizing the standardized schemes for metadata, we used the *MedicalEntity* class to describe the anatomical structure or system involved in the therapy simulated. To link the simulated data with datasets containing information about absorbed, equivalent, or effective doses calculated in gray or sievert correspondingly, we made use of the *includedInDataCatalog* property of the *MedicalIntangible* schema. To provide a more comprehensive and interoperable description, we are developing a new Meiga vocabulary (*Meiga*: :), which leverages the Radiation Oncology Ontology (Deckker et al. 2022) to extend the current schema with additional properties required for these computations. With this extension, we will be able to produce a richer and more standardized description, facilitating the interoperability and reusability of the data generated by our simulations.

3 EXPERIMENTATION AND DISCUSSION OF RESULTS

For testing the functionality of *RadPhantom*, different sets of trials were executed. These tests were performed using four different types of primary radiation: gamma rays, electrons, protons, and carbon ions. To assess and compare the results and performance of our implementation with the original phantom implementations, an incident radiation beam of 10^5 particles was generated at the coordinates (8.00, -13.57, 43.60) cm related to a cartesian coordinated system placed in the geometric center of the phantom. It should be noted that the positive X coordinates are oriented towards the left of the phantom's center.

As an example of *RadPhantom* capabilities, Figure 2 illustrates the trajectory of proton beams along the Y-axis (sagittal axis) in a positive direction, from the front to the back. These three images demonstrate the distribution of absorbed dose across sections along the longitudinal axis of the Reference Adult Male model (slices). Primary and secondary particles, resulting from interactions with the material, deposit energy in the tissues and organs during their propagation through the interior of the phantom. It can be observed that for the proton beam, the spatial distribution of the absorbed dose within the body follows the expected behavior. The dose is highly concentrated along the beam trajectory close to the injection point (slice 165 at 43.6 cm from the origin), and it becomes increasingly dispersed as we move away to the adjacent slices. These results were also compared with the corresponding ones obtained with the original phantom implementation. While no differences were observed in the deposited dose, an improvement of up to 20% was observed in the total time needed for completion when comparing the cloud-based performance of *RadPhantom* with the corresponding Geant4-based implementation.

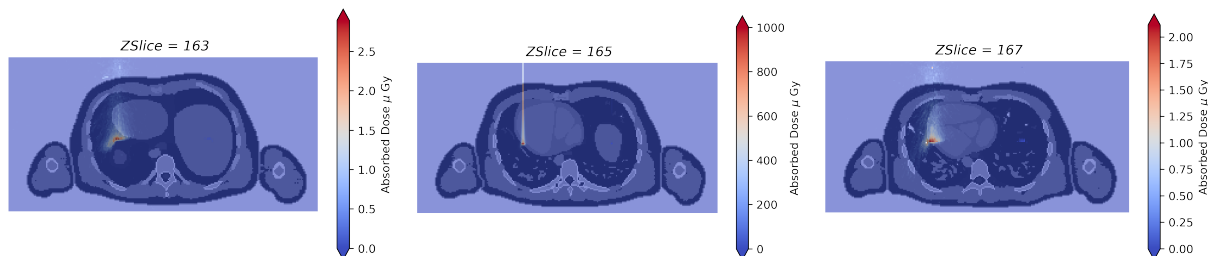


Figure 2: Two-dimensional map of the absorbed dose deposited in three different slices when the phantom is exposed to a beam of 10^5 protons of 125 MeV of kinetic energy. These results were obtained using the new *RadPhantom* cloud-based application.

As another benchmark of the developed application, we obtained the dose deposition in the beam direction, as illustrated in Fig. 3. This figure displays the absorbed dose as a function of depth for four distinct tests conducted using the *RadPhantom* application. We conducted three validation tests, each differing in the nature of a beam of 10^5 incident particles: photons (with an energy range from 1 MeV to 15 MeV), electrons (with an energy range from 5 MeV to 20 MeV), and protons (with an energy range from 50 MeV to 125 MeV). Air, being the initial medium with which the particles interact outside the phantom, is included in the simulations. However, it is not factored into the dose calculation, as it is naturally present.

The absorbed dose per particle as a function of depth was calculated by summing all doses in each plane along the voxelized Y-axis. This was achieved by integrating the dose in the X and Z directions:

$$D(y) = \sum_1^{NVoxelX} \sum_1^{NVoxelZ} D_{voxel}(x, z, y), \quad (1)$$

In this equation, $D_{voxel}(x, z, y)$ represents the dose deposited in each voxel. This value is obtained directly from the three-dimensional mesh output file resulting from the application. Meanwhile, D signifies the total dose in the cortical plane, which varies depending on the distance Y , on the sagittal axis (from the front to the back of the phantom). The variables $NVoxelX$ and $NVoxelZ$ denote the total number of voxels in the X and Z axis directions, respectively.

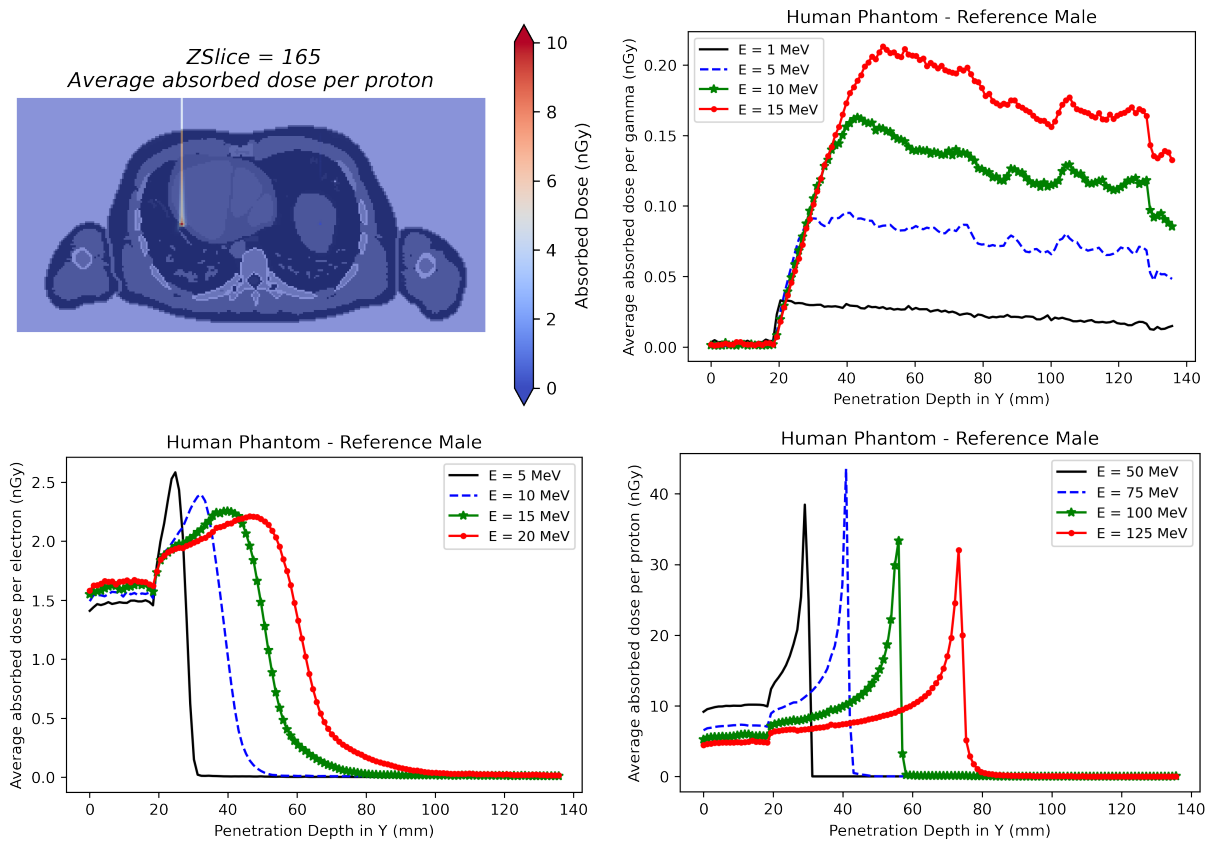


Figure 3: Presented are the results of twelve tests conducted using the new RadPhantom application, illustrating the absorbed dose as a function of depth. Top-left: The trajectory of the 10^5 incident particles beam in the Reference Adult Male model, identified by the total absorbed dose per voxel. Top-right: The photon beam with an energy range from 1 MeV to 15 MeV. Bottom-left: The electron beam with an energy range from 5 MeV to 20 MeV. Bottom-right: The proton beam with an energy range from 50 MeV to 125 MeV. The outcomes align with the distribution of different tissues and are consistent with results obtained using conventional tools.

Our findings depict the variation of the absorbed dose as a function of depth in the human phantom for each type of radiation, aligning with the anticipated profile of the deposited energy as a function of the distance. We subsequently compared these results with the corresponding outputs from the original applications. No differences were observed. Furthermore, the computations, when performed in a similar

computing power environment, required 20% less time to complete, thereby scoring the efficiency of our approach.

In the case of photons, we noted that the deposition of the average absorbed dose per particle gradually increases as the radiation penetrates the phantom, reaching a peak at a certain depth that depends on the photon energy. This pattern is representative of the typical interactions of photons with tissues, where processes such as the photoelectric effect, Compton scattering, and pair creation (for $E_\gamma > 2, m_e c^2$) transpire. It's worth noting that for tissues, Compton scattering is the dominant effect at these energy ranges. Interestingly, each graph exhibits minor fluctuations (small peaks) along the depth in the curves, attributable to radiation interactions with tissues of diverse densities.

Conversely, the rate of increase for electrons can be more pronounced compared to photons. This is attributable to the stronger interaction of electrons with tissues, a consequence of their electrical charge. As the energy of the beam escalates, the secondary photons, which result from the deceleration of energetic electrons (a process known as Bremsstrahlung), gain the capacity to penetrate deeper into the human phantom. This phenomenon is clearly visible in the bottom-left panel of Fig. 3, where the absorbed dose per electron at the peak becomes less steep at higher energies than for the $E_e = 5$ MeV beam.

Finally, the bottom-right panel depicts the average absorbed dose per proton. As expected, the total range is directly correlated with the beam energy. As protons penetrate the tissues, they decelerate, and the energy deposition per unit length escalates, reaching its zenith at very low energies. This behavior results in a maximum energy reservoir known as the Bragg peak, which is distinctly visible for all the proton beams. The disparities between the peaks align with the changes in densities as the beam infiltrates different tissues of varying densities. The position of the Bragg peak also concurs with the expected depth obtained by analytical and other Monte Carlo methods.

To assess the capabilities of RadPhantom in simulating the effects of ion beams, we also injected a beam of 12-C ions with 138.33 MeV/nucleon (1,660 MeV) of kinetic energy at the same location in the Reference Adult Male. The resulting absorbed dose $D(y)$ deposition as a function of depth (as per equation (1)) is depicted in the left panel of Fig. 4. When compared with other particles, larger absorbed doses per ion can be observed, reaching nearly $\lesssim 1 \mu\text{Gy}$ per particle per voxel in the Bragg peak region. For comparison, the resulting $D(y)$ for the proton beam of 75 MeV is displayed in the right panel of the same figure, showing a similar range in the body of about 40 mm, but with a total absorbed dose of ~ 50 nGy per proton per voxel at the peak. Due to their higher mass and charge, carbon ions exhibit a steeper Bragg peak than protons, indicating a higher linear energy transfer (LET) and a greater relative biological effectiveness (RBE) compared to protons. The results were cross-verified with standard tools, and no discrepancies were observed.

Once the absorbed dose is determined, both the equivalent dose per organ and the effective dose for the entire phantom can be calculated. To achieve this, we utilize the radiation weighting factors (a measure of the specific RBE for each type of particle) and the tissue weighting factors (a factor by which the equivalent dose to a tissue or organ is multiplied). These factors are provided by ICRP publications 60 (Clarke et al. 1990) and 147 (Harrison et al. 2021a; Harrison et al. 2021b). In Table 1, the results of these calculations are presented for the photon, electron, and proton beams previously described. Consistent with the absorbed dose values, the calculated effective dose values also increase with increasing energy. Comparisons are feasible as all the beams were injected at the same location in the Reference Adult Male phantom model.

The previously described virtual cluster completed all these tests in just 64 CPU-hours, which is noteworthy considering that the processors used are not the latest generation available. In addition, a significant time reduction of approximately 20% was observed compared to the performance of currently available tools. Furthermore, no discrepancies were found between the obtained results, confirming the accuracy of the simulated outcomes. These findings not only highlight the precision of the results from a physics standpoint but also emphasize the practicality and efficiency of the RadPhantom application for simulating radiation within voxelized phantoms.

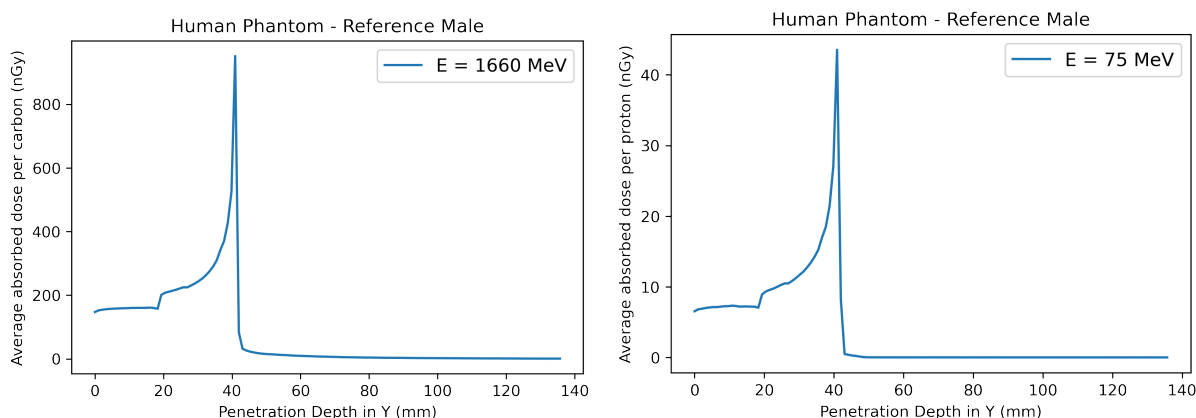


Figure 4: Displayed is the absorbed dose $D(y)$ as a function of penetration depth for a 10^5 beam of 12-C ions with 138.33 MeV/nucleon (1,660 MeV) of kinetic energy (left), and a 10^5 proton beam of 75 MeV (right). Despite the range in the body being quite similar, significant differences are observed in the absorbed dose per voxel per particle, highlighting the interaction characteristics of these two types of particles.

Table 1: Presented are the effective doses obtained from the injection of 10^5 particle beams at the same location in the Reference Adult Male phantom model, as simulated using the new RadPhantom application. The table provides a comprehensive comparison of the results for different types of radiation.

Photons	Dose [μ Sv]	Electrons	Dose [μ Sv]	Protons	Dose [μ Sv]
E = 1 MeV	27	E = 5 MeV	219	E = 50 MeV	4897
E = 5 MeV	89	E = 10 MeV	464	E = 75 MeV	7404
E = 10 MeV	144	E = 15 MeV	763	E = 100 MeV	9766
E = 15 MeV	193	E = 20 MeV	1012	E = 125 MeV	12460

To ensure the reproducibility and standardization of the simulations, we developed an extended vocabulary schema based on current standards, as described in section 2. In addition to utilizing DICOM images and reference computational phantoms, our approach incorporates metadata, ontologies, and persistent identifiers to ensure that the data generated by our simulations are easily discoverable, accessible, and reusable, thus adhering to the FAIR (Findable, Accessible, Interoperable, and Reusable) paradigm. By leveraging virtualized containers, we can take advantage of the scalability and flexibility offered by federated clouds such as the European Open Science Cloud, as well as public cloud platforms like Amazon Web Services or Google Cloud, thus enabling wider accessibility of the RadPhantom application to the scientific community at large.

4 CONCLUSIONS AND FUTURE WORK

In this work, we presented the development and initial evaluation of the RadPhantom application, integrated within the Meiga framework. The application allows for the simulation of radiation-matter interactions in anthropomorphic phantoms. By voxelizing the subject’s DICOM images or utilizing existing voxelized models, personalized phantom models can be generated, providing a modular and adaptable approach. Leveraging the capabilities of Meiga, the application facilitates large-scale simulations in cloud-based environments.

The functionality and efficiency of RadPhantom were demonstrated through a comprehensive set of tests involving various primary radiation types: photons, electrons, protons, and carbon ions. The obtained results were compared with those from original phantom implementations, revealing no discrepancies in the

calculated absorbed dose. The application exhibited remarkable performance, completing simulations 20% faster than existing tools. This efficiency was achieved by leveraging cloud-based resources and virtualized containers, enabling scalability and flexibility in the computing infrastructure.

The simulations conducted using RadPhantom consistently delivered accurate results. The absorbed dose distributions within the anthropomorphic phantoms exhibited the expected patterns for different radiation types. Additionally, the calculated effective doses, based on radiation tissue weighting factors recommended by current regulations, displayed the anticipated increasing trend with higher energy levels for all radiation types. These dose calculations provided valuable insights into the potential biological effects of the simulated radiation scenarios. The integration of standardized metadata, ontologies, and persistent identifiers ensured the reproducibility and standardization of the simulations, aligning with the FAIR principles.

The potential applications of this work are wide-ranging. One notable application lies in the evaluation of absorbed doses in medical scenarios. Furthermore, our approach can enhance the assessment of effective doses experienced during commercial flights and will be integrated into the next version of the ACORDE code (Asorey et al. 2023). We are also adapting this model for sitting and standing individuals on board commercial aircraft Geant-4 models, such as the Airbus A320 and A350. Moreover, our application can contribute to the evaluation of radiation shielding materials in rapid neutron production facilities and assess the effective dose for individuals in the event of severe accidents within these facilities.

ACKNOWLEDGMENTS

This work was partially supported by the computing facilities provided by CIEMAT and hosted in the Extremadura Research Centre for Advanced Technologies (CETA-CIEMAT, Turgalium supercomputer) and the Moncloa campus in Madrid (ACME and Xula supercomputers), with European Regional Development Fund (ERDF) funds. It was also partially co-funded by the Consejo de Seguridad Nuclear (CSN), Spain, under the NEREIDA project. MC wants to acknowledge support by the FEDER/Ministerio de Ciencia, Innovación y Universidades - Agencia Estatal de Investigación grant PID2020-112796RB-C22.

REFERENCES

- Agostinelli, S., J. Allison, K. Amako, J. Apostolakis, H. Araújo, P. Arce, M. Asai, D. Axen, S. Banerjee, G. Barrand, F. Behner, L. Bellagamba, J. Boudreau, L. Broglia, A. Brunengo, S. Chauvie, J. Chuma, R. Chytráček, G. Cooperman, and D. Zschiesche. 2003. "GEANT4—a Simulation Toolkit". *Nuclear Instruments and Methods in Physics Research Section A: Accelerators, Spectrometers, Detectors and Associated Equipment* 506(3):250–303.
- Allison, J., K. Amako, J. Apostolakis, P. Arce, M. Asai, T. Aso, E. Bagli, A. Bagulya, S. Banerjee, G. Barrand, B. Beck, A. Bogdanov, D. Brandt, J. Brown, H. Burkhardt, P. Canal, D. Cano-Ott, S. Chauvie, K. Cho, G. Cirrone, G. Cooperman, M. Cortés-Giraldo, G. Cosmo, G. Cuttone, G. Depaola, L. Desorgher, X. Dong, A. Dotti, V. Elvira, G. Folger, Z. Francis, A. Galoyan, L. Garnier, M. Gayer, K. Genser, V. Grichine, S. Guatelli, P. Guèye, P. Gumplinger, A. Howard, I. Hřivnáčová, S. Hwang, S. Incerti, A. Ivanchenko, V. Ivanchenko, F. Jones, S. Jun, P. Kaitaniemi, N. Karakatsanis, M. Karamitros, M. Kelsey, A. Kimura, T. Koi, H. Kurashige, A. Lechner, S. Lee, F. Longo, M. Maire, D. Mancusi, A. Mantero, E. Mendoza, B. Morgan, K. Murakami, T. Nikitina, L. Pandola, P. Paprocki, J. Perl, I. Petrović, M. Pia, W. Pokorski, J. Quesada, M. Raine, M. Reis, A. Ribon, A. Ristić Fira, F. Romano, G. Russo, G. Santin, T. Sasaki, D. Sawkey, J. Shin, I. Strakovsky, A. Taborda, S. Tanaka, B. Tomé, T. Toshito, H. Tran, P. Truscott, L. Urban, V. Uzhinsky, J. Verbeke, M. Verderi, B. Wendt, H. Wenzel, D. Wright, D. Wright, T. Yamashita, J. Yarba, and H. Yoshida. 2016. "Recent developments in Geant4". *Nuclear Instruments and Methods in Physics Research Section A: Accelerators, Spectrometers, Detectors and Associated Equipment* 835:186–225.
- Asorey, H., M. Suárez-Durán, and R. Mayo-García. 2023. "ACORDE: A New Application for Estimating the Dose Absorbed by Passengers and Crews in Commercial Flights". *Applied Radiation and Isotopes* 196:110752.
- Bertolli, C. P., C. Sarmiento-Cano, and H. Asorey. 2022. "Estimation of the Muon flux Expected at the ANDES Underground Laboratory". *Anales de la Asociación de Física Argentina (AFA)* 32(4):106–111.
- Brickley, D. and others. 2022. "Schema.org". <https://schema.org/>, accessed: 01.05.2023.
- Brun, R., and F. Rademakers. 1997. "ROOT—An Object Oriented Data Analysis Framework". *Nuclear Instruments and Methods in Physics Research Section A: Accelerators, Spectrometers, Detectors and Associated Equipment* 389(1-2):81–86.

- Calderón-Ardila, R., H. Asorey, A. Almela, A. Sedoski, C. Varela, N. Leal, and M. Gómez-Berisso. 2022. “Development of Mudulus, a Muography Detector Based on Double-Synchronized Electronics for Geophysical Applications”. *Journal for Advanced Instrumentation in Science* 2022(1):1–5.
- Caon, M. 2004. “Voxel-Based Computational Models of Real Human Anatomy: A Review”. *Radiation and Environmental Biophysics* 42:229–235.
- Clarke, R. H., C. Dunster, and L. Guskova. 1990. “ICRP 60: The 1990 Recommendations of the International Commission on Radiological Protection”. *Annals of the International Commission on Radiological Protection* 21:1–211.
- Clement, C. 2009. “ICRP 110: Adult Reference Computational Phantoms”. *Annals of the International Commission on Radiological Protection* 39:165.
- Costa, G. C., L. V. D. Sa, and D. A. Bonifacio. 2015. “Application of GATE/Geant4 for Internal Dosimetry Using Male ICRP Reference Voxel Phantom by Specific Absorbed Fractions Calculations for Photon Irradiation”. *Biomedical Physics and Engineering Express* 1:045201.
- Deckker, A. and others 2022. “Radiation Oncology Ontology - ROO”. <https://www.cancerdata.org/roo-information>, accessed: 01.05.2023.
- Dewji, S. A., N. Bhakta, A. J. Davis, and K. F. Eckerman. 2004. “The ORNL Mathematical Phantom Series”. *Health Physics* 87:530–546.
- Franck, D., L. Laval, N. Borissov, P. Guillerme, and J. M. Bordy. 2001. “Development of Voxelised Numerical Phantoms Using MCNP Monte Carlo Code: Application to in Vivo Measurement”. *Article Radioprotection* 36:77–86.
- Guatelli, S., B. Mascialino, M. G. Pia, and W. Pokorski. 2006. “Geant4 Anthropomorphic Phantoms”. In *2006 Institute of Electrical and Electronics Engineers Inc. Nuclear Science Symposium Conference Record*, Volume 3, 1359–1362. Institute of Electrical and Electronics Engineers Inc. Xplore: Institute of Electrical and Electronics Engineers Inc.
- Harrison, J., M. Balonov, F. Bochud, C. Martin, H.-G. Menzel, P. Ortiz-Lopez, R. Smith-Bindman, J. Simmonds, and R. Wakeford. 2021a. “ICRP 147: Use of Dose Quantities in Radiological Protection”. *Annals of the The International Commission on Radiological Protection* 50:9–82.
- Harrison, J., M. Balonov, F. Bochud, C. Martin, H.-G. Menzel, P. Ortiz-Lopez, R. Smith-Bindman, J. Simmonds, and R. Wakeford. 2021b. “The Use of Dose Quantities in Radiological Protection: ICRP Publication 147 Ann ICRP 50(1) 2021”. *Journal of Radiological Protection* 41:410–422.
- Large, M. J., A. Malaroda, M. Petasecca, A. B. Rosenfeld, and S. Guatelli. 2020, oct. “Modelling ICRP110 Adult Reference Voxel Phantoms for Dosimetric Applications: Development of a New Geant4 Advanced Example”. *Journal of Physics: Conference Series* 1662:012021.
- Martins, M. C., T. P. Cordeiro, A. X. Silva, D. Souza-Santos, P. Queiroz-Filho, and J. Hunt. 2014. “Dose Conversion Coefficients for ICRP110 Voxel Phantom in the Geant4 Monte Carlo Code”. *Radiation Physics and Chemistry* 95:309–312.
- Pagano, D., G. Bonomi, A. Donzella, A. Zenoni, G. Zumerle, and N. Zurlo. 2021. “EcoMug: an Efficient COsmic MUon Generator for Cosmic-Ray Muon Applications”. *Nuclear Instruments and Methods in Physics Research Section A: Accelerators, Spectrometers, Detectors and Associated Equipment* 1014:165732.
- Rubio-Montero, A., R. Pagán-Muñoz, R. Mayo-García, A. Pardo, I. Sidelnik, and H. Asorey. 2021. “A Novel Cloud-Based Framework for Standardized Simulations in the Latin American Giant Observatory (LAGO)”. In *Proceedings of the 2021 Winter Simulation Conference*, edited by S. Kim, B. Feng, K. Smith, S. Masoud, Z. Zheng, C. Szabo, and M. Loper, 1–12. Piscataway, New Jersey: Institute of Electrical and Electronics Engineers, Inc.
- Rubio-Montero, A., R. Pagán-Muñoz, R. Mayo-García, A. Pardo-Díaz, I. Sidelnik, and H. Asorey. 2021. “The EOSC-Synergy Cloud Services Implementation for the Latin American Giant Observatory (LAGO)”. In *Proceedings of 37th International Cosmic Ray Conference*, 1–4. Institute of Electrical and Electronics Engineers, Inc.: Sissa Medialab.
- Sarmiento-Cano, C., M. Suárez-Durán, R. Calderón-Ardila, A. Vásquez-Ramírez, A. Jaimes-Motta, L. A. Núñez, S. Dasso, I. Sidelnik, and H. Asorey. 2022. “The ARTI Framework: Cosmic Rays Atmospheric Background Simulations”. *The European Physical Journal C* submitted:1019.
- Sarrut, D., N. Arbor, T. Baudier, D. Borys, A. Etxebeste, H. Fuchs, J. Gajewski, L. Grevillot, S. Jan, G. C. Kagadis, H. G. Kang, A. Kirov, O. Kochebina, W. Krzemien, A. Lomax, P. Papadimitroulas, C. Pommeranz, E. Roncali, A. Rucinski, C. Winterhalter, and L. Maigne. 2022. “The OpenGATE Ecosystem for Monte Carlo Simulation in Medical Physics”. *Physics in Medicine & Biology* 67(18):184001.
- Sato, K., H. Noguchi, Y. Emoto, S. Koga, and K. Saito. 2007. “Japanese Adult Male Voxel Phantom Constructed on the Basis of CT Images”. *Radiation Protection Dosimetry* 123:337–344.
- Sempau, J. 2002. “Monte Carlo Simulation for Radiation Transport. Applications in Medical Physics”. *Radioprotection* 31:18–26.
- Taboada, A., C. Sarmiento-Cano, A. Sedoski, and H. Asorey. 2022. “Meiga, a Dedicated Framework Used for Muography Applications”. *Journal for Advanced Instrumentation in Science* 2022(1):266.
- Tanaka, H. K. 2022. “Principles of Muography and Pioneering Works”. *Muography: Exploring Earth’s Subsurface with Elementary Particles* 270:1–17.

AUTHOR BIOGRAPHIES

OSIRIS NÚÑEZ-CHONGO (osirsnunez93@gmail.com) is a master's student in the Interuniversity Master's in Industrial Mathematics at the Universidad Carlos III of Madrid. She obtained her Master of Engineering in Nuclear and Energy Facilities from the Higher Institute of Applied Sciences and Technologies (2021), after completing her Bachelor of Engineering in Nuclear and Energy Technologies in (2016) at the same institute. She participates in a research project in medical collaboration with the National Institute of Ophthalmology of Cuba. Her research focuses on mathematical modeling and development of numerical simulations. Her work is focused on the study of biomechanical models for medical applications and interaction simulations of high doses of radiation with the subject. She has collaborated on 5 articles of scientific relevance.

MANUEL CARRETERO (manili@math.uc3m.es) is Associate Professor of Mathematics at the University Carlos III de Madrid (UC3M), Director-UC3M of the Inter-university Master in Industrial Mathematics and former sub-director of the University Institute "Gregorio Millán Barbany" for Modelling and Simulation in Fluidynamics, Nanoscience and Industrial Mathematics. He earned his PhD in Mathematics from UC3M (2002) and he won the PhD Extraordinary Award granted by UC3M (2005). His research in Applied Mathematics covers several areas: Computational methods in Biology and Physics, numerical methods, asymptotic and nonlinear analysis, multiscale problems, charge and spin transport in nanostructures, chaos, combustion and detonations. He authored 47 scientific publications, 39 articles (27 of them indexed Q1 in JCR) and 8 chapters of scientific books. He has participated as researched on 9 projects and as a principal researcher on 2. He has supervised 3 PhD theses and 8 Master's theses.

RAFAEL MAYO-GARCÍA (rafael.mayo@ciemat.es) is a senior researcher at CIEMAT, Harvard University Fellow, and coordinator of the European EERA Joint Programme 'Digitalisation for Energy'. He earned his PhD in Physics from Universidad Complutense de Madrid (2004). He has been involved in many experiments in the US, Bulgaria, Sweden, and Ireland (funded, among others, by the European Commission with a Marie Curie Action). He has also obtained a postdoctoral fellowship in the Spanish Juan de la Cierva Programme. He authored more than 160 scientific articles. He has participated in 64 projects (being PI in 9 out of them) and has been involved in several European and National initiatives working on HPC & BD scientific developments. He also has served several institutions as an evaluator for their competitive Calls, European Commission included and has supervised 8 theses.

HERNÁN ASOREY (hernan.asorey@iteda.cnea.gov.ar) is a senior researcher in CNEA, Argentina. He is also an Associated Professor at UNRN in Argentina. He earned his PhD in Physics from Instituto Balseiro (2012), after completing his MSc in Particles and Fields (2005) at the same institute. He participates in LAGO, Auger and ANDES collaborations, and currently, he is the project manager of the PlomBOX project, funded by the GCRF-UKRI fund to produce synthetic biosensors for the detection of lead in drinkable water, and he is leading a research group focusing on the design and development of novel particle detectors for geophysical and industrial applications. His research covers a broad range of areas, and his work is oriented to the simulation of the interaction of radiation with matter. He successfully advised 2 postdoctoral researchers, 5 PhD theses, 5 MSc theses and 7 undergraduate theses in 4 countries. He has authored or co-authored more than 136 articles, 1 textbook in elementary physics, 1 international patent and more than 100 proceedings and technical reports.